ACS APPLIED MATERIALS & INTERFACES

Research Article

www.acsami.org

Tapered Optical Fiber Probe Assembled with Plasmonic Nanostructures for Surface-Enhanced Raman Scattering Application

Zhulin Huang,[†] Xing Lei,[§] Ye Liu,[§] Zhiwei Wang,[†] Xiujuan Wang,[†] Zhaoming Wang,[†] Qinghe Mao,[§] and Guowen Meng*[,†,‡]

[†]Key Laboratory of Materials Physics and Anhui Key Laboratory of Nanomaterials and Nanotechnology, Institute of Solid State Physics, Chinese Academy of Sciences, Hefei 230031, P. R. China

[‡]University of Science and Technology of China, Hefei 230026, P. R. China

[§]Anhui Provincial Key Laboratory of Photonics Devices and Materials, Anhui Institute of Optics and Fine Mechanics, Chinese Academy of Sciences, Hefei 230031, P. R. China

Supporting Information

ABSTRACT: Optical fiber-Raman devices integrated with plasmonic nanostructures have promising potentials for *in situ* probing remote liquid samples and biological samples. In this system, the fiber probe is required to simultaneously demonstrate stable surface enhanced Raman scattering (SERS) signals and high sensitivity toward the target species. Here we demonstrate a generic approach to integrate presynthesized plasmonic nanostructures with tapered fiber probes that are prepared by a dipping–etching method, through reversed electrostatic attraction between the silane couple agent modified silica fiber probe and the nanostructures. Using this approach, both negatively and positively charged plasmonic nanostructures with various morphologies (such as Au nanosphere, Ag nanocube, Au nanorod, Au@Ag core–shell nanorod) can be stably assembled on the tapered silica fiber probes. Attributed to the electrostatic force between the plasmonic units and the fiber surface, the nanostructures do not disperse in liquid samples easily, making the relative standard deviation of SERS signals as low as 2% in analyte solution. Importantly, the detection sensitivity of the system can be optimized by adjusting the cone angle (from 3.6° to 22°) and the morphology of nanostructures assembled on the fiber. Thus, the nanostructures-sensitized optical fiber-Raman probes show great potentials in the applications of SERS-based environmental detection of liquid samples.

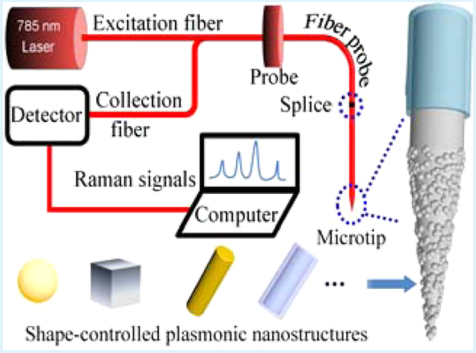

KEYWORDS: *plasmonic nanostructures, tapered fiber probe, electrostatic attraction, surface-enhanced Raman scattering, detection*

1. INTRODUCTION

Optical fiber-Raman sensors integrated with plasmonic nanostructures have potentials in surface-enhanced Raman scattering (SERS) based monitoring of remote liquid species and biological species.[1,2] In a typical optical Raman-fiber setup, a single fiber transmits both the exciting laser and the Raman scattered signals that are collected from the SERS-active surface bound to the fiber tip.[3−5] Such SERS-active tips incorporated with plasmonic nanostructures are usually prepared by a traditional dip-coating method.[6,7] However, the plasmonic nanostructures assembled on the fiber probes with this method tend to disperse in liquid samples, leading to unstable SERS signals in practical detection. To solve this problem, physical vapor deposition[7,8] and laser-induced chemical deposition[9−11] have been developed. Nevertheless, these approaches are either expensive or could not rationally tailor the shape, size, and distribution of the nanostructures, thus limiting the actual SERS-sensitivity of the fiber probe. It is known that the electric field enhancement generated by illuminated noble metal nanoparticles is largely dependent on the particle geometry,[12] which then directly dictates the coupling between the surface plasmon resonance (SPR) of nanoparticles and the excitation laser.[13] For practical SERS-active fiber probes, the plasmonic nanostructures decorated on the fiber surface should not only be stable in liquid samples, but also provide a high SERS-sensitivity for analyte detection.

With the development of solution phase synthetic techniques, noble metal nanostructures with varied shapes (spheres,[14] cubes,[15−17] rods,[18] triangles,[19] stars,[20] and polyhedra[21]) and distinct SPR can be achieved. Most of the shape-controlled synthetic procedures involve the reduction of salt precursors in the presence of surfactants, polymers, biomacromolecules, coordinating ligands, and sometimes with the mediation of ionic species. On one hand, such nanostructures are featured by sharp edges that can provide strong localized electron oscillation for large electromagnetic enhancement. On the other hand, these plasmonic nanostructures usually carry surface charges (either negative or positive) induced by

Received: May 14, 2015
Accepted: July 17, 2015
Published: July 17, 2015

DOI: 10.1021/acsami.5b04202
ACS Appl. Mater. Interfaces 2015, 7, 17247−17254

surfactants, such as poly(vinylpyrrolidone), citrate, cetyltrimethylammonium bromide (CTAB) and hexadecyl trimethylammonium chloride (CTAC), etc. Importantly, the plasmon bands of such Au/Ag nanoparticles synthesized by the above-mentioned approaches can be tuned from near-infrared to visible regions,[22] showing promising applications in SPR-based sensors.[23] Regarding the assembly of SERS-active nanostructures onto the silica surface of fiber probe, electrostatic attraction has shown great potential. For example, by using contrary surfactants, Au-nanorods have been assembled onto Ag-nanowires[24] and citrate stabilized Au-nanoparticles can be decorated onto silicon wafer.[25] However, the assembly of the above shape-controlled plasmonic nanostructures with fiber probes via electrostatic attraction is largely unexplored. In this context, investigation of the assembly of varied plasmonic nanostructures onto fiber probes and the performance of the fiber SERS probes is an important step to realize an efficient, stable and sensitive optical fiber sensor for detection application.

It is known that silane couple agent can be readily modified onto the silica surface and its bifunctional groups can provide exerted groups such as amino and carboxyl to accommodate charged plasmonic nanostructures.[26,27] Herein, on the basis of electrostatic attraction by using silane couple agents, we present a facile and effective approach to the incorporation of noble metal nanostructures with tunable shape and size onto the surface of tapered fiber probes for SERS-based detection, as schematically shown in Figure 1. Either negatively or positively charged nanostructures of noble metals (such as Au, Ag) with various morphologies (such as nanosphere, nanocube, nanorod, core−shell nanorod) could be uniformly and stably assembled

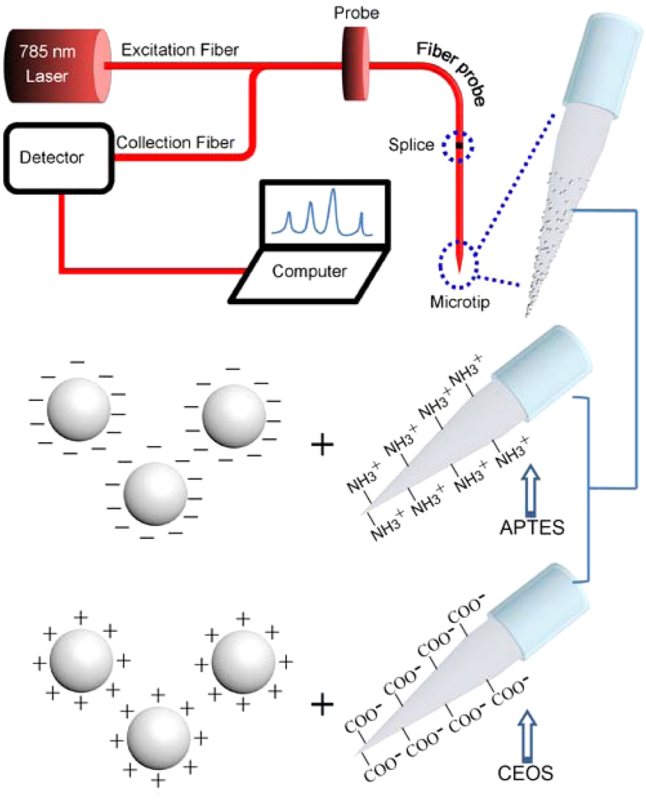

Figure 1. Schematical diagram showing the fiber Raman experimental setup and the electrostatic attraction dominated assembly of charged noble metal nanoparticles onto reversely charged tapered fiber probe.

on the 3-aminopropyl trimethoxysilane (APTES) or carboxyethyl silanetriol sodium (CEOS) decorated tapered fiber probes with controlled packing densities. By using *para*-aminothiophenol (*p*-ATP) and methyl-parathion (MP) as probe molecules, the relative standard deviation (RSD) of the SERS signals can be down to 2% tested in analyte solution, showing excellent signal stability in liquid samples. Also, the taper angle of the fiber probe and the SPR properties of the nanostructures can be tailored to optimize the detection sensitivity. Our assembly scheme can be exploited to other versatile nanostructures-sensitized SERS fiber probes of different optical fiber type, showing great potentials in high quality nanostructures-sensitized SERS fiber probe sensors.

2. EXPERIMENTAL SECTION

2.1. Materials. Chloroauric acid, silver nitrate, sodium citrate, ascorbic acid (AA), sodium chloride, hydrofluoric acid, dimethylformamide (DMF), and ethanol were purchased from Sinopharm Chemical Reagent limited corporation. Poly(vinylpyrrolidone) (PVP-K29, (C6H9NO)n, Mw=58000), CTAB, CTAC APTES (98%, ethanol), CEOS (25%, water), pentanediol, 2-Naphthalenethiol (2-NAT), *p*-ATP, and methyl parathion were obtained from Aladdin. Milli-Q deionized (DI) water (resistivity =18.2 MΩcm^{-1}) was used for all preparations.

2.2. Fabrication of charged plasmonic nanostructures. Negatively charged Ag nanocubes. PVP protected Ag nanocubes were fabricated by using a polyol reduction of silver ions in the presence of Cl^-.[28] Hydroxyl group terminated PVP was used as the surfactant to kinetically mediate the particle shape. At the reaction temperature (~150 °C), the hydroxyl groups of PVP finally evolved into carboxyls,[29] which can readily ionize the H^+ and expose the negatively charged carboxylate radicals.

Negatively charged Au-nanospheres. Citrate stabilized Au-nanospheres were prepared by reducing auric chloride acid (200 μL, 25 g/L) using trisodium citrate (1000 μL, 10 g/L). The reaction temperature was above 90 °C by means of oil bath. The diameter of the citrate stabilized Au-nanospheres is about 13 nm.

Positively charged Au-nanorods. Au-nanorods were prepared by a seed mediated growth process with modifications from previous reports in three steps.[30] First, Au seed solution was prepared as follows. $HAuCl_4$ solution (0.01 M, 0.25 mL) was mixed with CTAB solution (0.1 M, 9.75 mL). Subsequently, ice-cold $NaBH_4$ solution (0.01 M, 0.6 mL) was added to the mixed solution. The seed solution was stirred vigorously (800 rpm) for 120 s and further settled in a water bath (26 °C) for 2 h. The solution color changed into brown, indicating the formation of Au seeds. The next step is the growth of Au-nanorods. Aqueous solutions of $HAuCl_4$ (0.01 M, 0.25 mL), $AgNO_3$ (0.01 M, 0.4 mL), and HCl (1.0 M, 0.8 mL) were injected into CTAB solution (0.1 M, 40 mL) and shaken in turn. The mixture was then added with aqueous AA solution (0.1 M, 0.32 mL) and shaken for 30 s. Normally, the orange color of the mixture became transparent. Subsequently, Au seed solution (0.096 mL) was injected in the mixture solution, shaken for 30 s and settled in water bath (28 °C) overnight. In this way, Au-nanorods with aspect ratio about 4−5 were obtained.

Positively charged Au@Ag core−shell nanorods. Au@Ag core−shell nanorods were prepared by wrapping Ag shell on the Au-nanorods,[31] so that the SPR bands can be readily tuned. The CTAB stabilized Au-nanorods (30 mL) were first treated with a subsurfactant procedure with CTAC, by three cycles of centrifugation-adding CTAC (80 mM)-sonication. The CTAC protected Au-nanorods (30 mL) were added with $AgNO_3$ (0.01 M, 2.5 mL), AA (0.1 M, 2.5 mL). The mixture was shaken and placed in a water bath (70 °C) for 3 h to achieve the Ag-shell wrapped Au-nanorods. To be noted, the Ag-shell thickness can be readily tuned by adjusting the Ag/Au concentration ratio, e.g., by adding different volumes of $AgNO_3$ solution (0.2 mL, 0.5 mL, 1 mL, 1.5 mL, etc.). The as-prepared Au@Ag core−shell nanorod solutions

DOI: 10.1021/acsami.5b04202
ACS Appl. Mater. Interfaces 2015, 7, 17247−17254

were finally centrifugated and washed with DI water repeatedly to remove the most CTAC surfactant and reserved.

2.3. Fabrication of nanostructures-sensitized tapered fiber probe. The tapered fiber probes were prepared by etching naked fiber in hydrofluoric acid. Briefly, multimode silica-based fiber with core (200 μm) and cladding (220 μm) was used. The cladding of the fiber ends was peeled off by using a blade. The hydrofluoric acid solution (40%) was sealed with methyl silicone oil to prevent volatilization. The cone angle of the fiber taper was adjusted by tuning the upward pulling speed along the fiber axis of a pulling machine. When the upward pulling speed is zero, the cone angle of the bare fiber taper is 22° due to the liquid surface tension. Otherwise, by changing the pulling speed of the apparatus, other cone angle of 3.6° (19.5 μm/min), 5.6° (11.8 μm/min), 8.2° (6 μm/min), 11.6° (3.7 μm/min), and 16° (1.6 μm/min) can be obtained. The presynthesized noble metal nanoparticles were subsequently decorated on the tapered fiber probe using silane couple agent (either APTES or CEOS) functionalized fiber probes according to the following procedure. The freshly prepared tapered fiber probe with abundant hydroxyl groups hung on the silica surface was dipped in aqueous solution of APTES (5 μL/mL) or aqueous solution of CEOS (20 μL/mL). After 30 min, the fiber probe was taken out, rinsed with DI water, and dipped into reversely charged nanostructure suspensions for 4 h to realize a saturated adsorption of the nanostructures.

2.4. Characterizations. The morphologies of the nanostructures were characterized by using scanning electron microscope (SEM, Hitachi SU8020) and transmission electron microscope (TEM, JEOL 2010). The optical absorbance of the nanostructures was measured by using ultraviolet−visible-near-infrared spectrophotometer (Varian, Cary 500). For fiber-Raman measurements, the nanostructures-assembled tapered fiber probes were directly dipped in analyte solutions, and excited at 785 nm laser with an acquisition time 2 s. Or else, the fiber probes were delt with a "dip and dry" process and tested in the air. All the laser power values stated in the experiments indicate the effective power emitted from the end of fiber.

3. RESULTS AND DISCUSSIONS

3.1. Assembling fiber surface with desired nanostructures via electrostatic attraction. Figure 1 schematically shows the fiber-Raman system and the electrostatic attraction induced assembly of nanostructures onto the surface of the tapered fiber probe. Here, we use multimode silica-based fiber with core (200 μm) and cladding (220 μm) as an example. Actually, other optical fibers such as single mode fiber and multimode fiber with different structural configurations are also applicable, due to the identical silica component. Briefly, a 785 nm exciting laser from the standard fiber probe of a portable spectrometer is coupled with one end of a 15 cm long transit multimode fiber. The other end is spliced to the tapered fiber probe, which is kept as long as 12 cm. Herein a tapered fiber probe is chosen, as it can provide a larger effective surface area to load plasmonic nanostructures illuminated by the evanescent wave and thus enhance the exciting laser power density threshold of the sample damage, so that the total SERS signals can be efficiently generated.[11] The fiber probe, due to the abundant hydroxyl groups exposed on the silica surface, can be easily decorated with silane coupling agent. In an aqueous environment, the silane coupling agent molecules ($YSiX_3$) are hydrolyzed to form silanol groups according to the following chemical reaction:

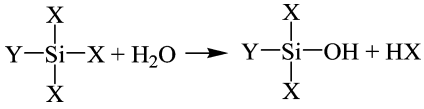

The products then shrink with the hydroxyls of the fiber probe:

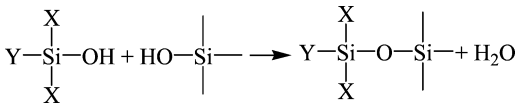

In organic solvent without H_2O, the hydrolyzable groups directly react with the surface silanols of the fiber probe:

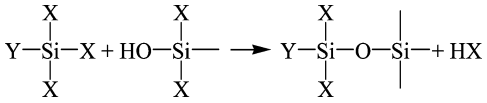

Herein X represents a hydrolyzable group, while Y can be NH_2, NaOOC, and SH functional groups. Take APTES ($NH_2(CH_2)_3$-Si-$(OC_2H_5)_3$) as an example; upon chemical decoration of APTES onto the fiber surface, the amino groups are exposed outside. The amino groups tend to draw H^+ in solution phase, subsequently affiliating the negatively charged nanostructures.[32] When immersed in nanostructure suspensions, the amino groups on the fiber surface function as bridges to draw the negatively charged nanostructures through electrostatic force. Whereas if CEOS ($NaOOC(CH_2)_2$-Si-$(OH)_3$) is decorated on the fiber surface, the carboxyls with negative charges directly adsorb positively charged nanostructures in solution, such as CTAB and CTAC protected Au-nanorods and Au@Ag core−shell nanorods.

3.2. Characterization of the tapered fiber probe assembled with plasmonic nanostructures. Figure 2 presents the optical images of APTES modified fiber probes of varied cone angles assembled with negatively charged Ag nanocubes (Figure 2a−f) and the scanning electron microscope (SEM) images of Ag nanocubes decorated on the fiber probe (Figure 2h, i). It is visualized that approximately the entire surface of the cone tips with varied taper angles is covered with a layer of Ag-nanostructures. For comparison, Figure 2g is a tapered fiber probe (8.2°) without the decoration of APTES. It is seen that no apparent nanostructure adsorption occurs. The SEM images indicate that a layer of incontinuous Ag nanocubes is irregularly distributed on the fiber probe (8.2°, Figure 2h, i). Further microscopic characterizations (see the SEM images in Figure S1 of the Supporting Information) show that, at the end of taper, where the diameter is ~5 μm, the density of nanoparticles is relatively low. At the cone neck where the diameter is ~200 μm, more intensive Ag nanocubes are assembled on the tapered fiber probe, due to the higher collision probability between the Ag nanocubes and the fiber probe. Actually, the packing density of the assembled nanostructures can be controlled by applying different immersion duration of fiber probe in the nanostructure suspension. Within 4 h, the amount of Ag nanocubes loaded on the fiber surface reaches saturation (see the SEM images in Figure S2). According to the principle of electrostatic attraction, other plasmonic nanostructures with negative charges can also be assembled on the APTES functionalized fiber probe; for example, citrate stabilized Au nanospheres also can be uniformly assembled on the tapered fiber surface (Figure 3).

For positively charged nanostructures, the fiber probes were modified with CEOS so that the surface of the fiber probe shows electronegativity. We first prepared highly monodis-

DOI: 10.1021/acsami.5b04202
ACS Appl. Mater. Interfaces 2015, 7, 17247−17254

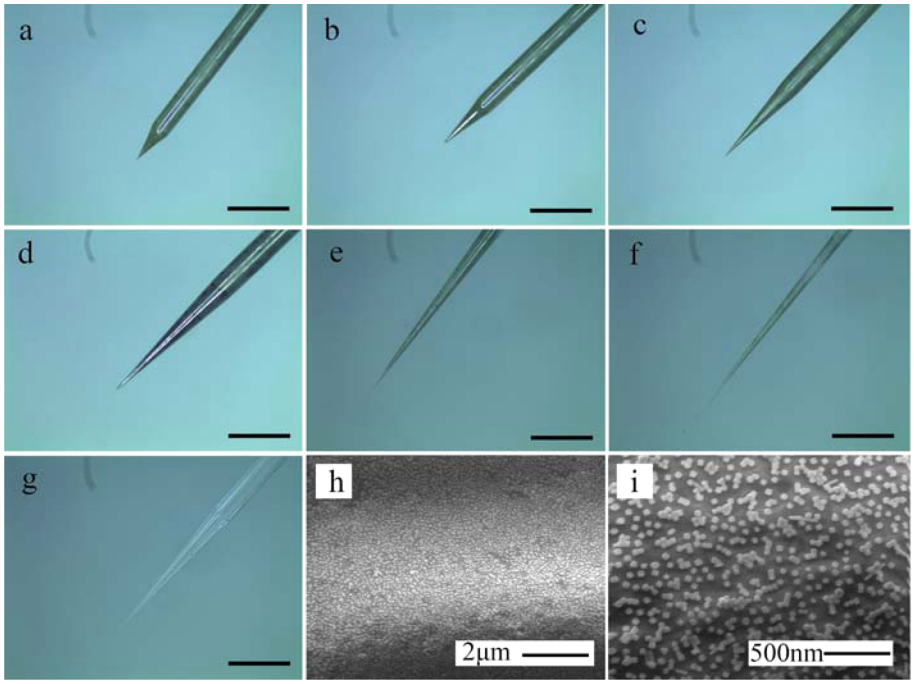

Figure 2. (a)−(f) Optical images of negatively charged Ag nanocubes decorated tapered fiber probes with varied cone angles of 22°, 16°, 11.6°, 8.2°, 5.6°, and 3.6°, respectively. (g) Optical image of a 8.2° tapered fiber probe without the functionalization of APTES but equal immersion time in a Ag-nanocube suspension. All the scale bars in the optical images indicate 600 μm. (h), (i) SEM images of a tapered fiber probe surface with Ag nanocubes.

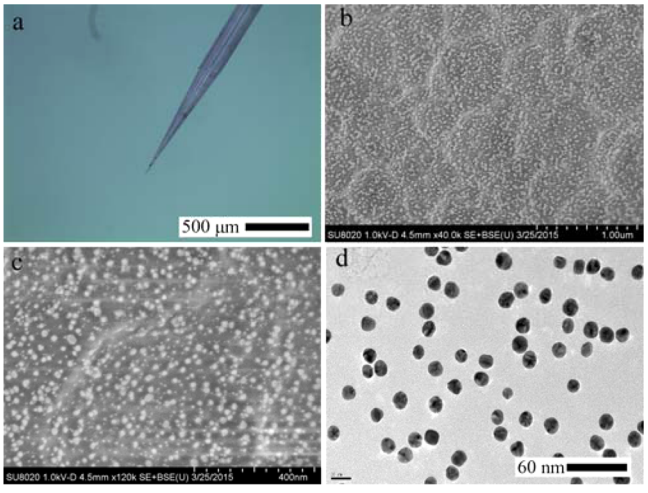

Figure 3. Citrate stabilized Au-nanospheres assembled on a 8.2° tapered fiber probe using APTES. (a) The optical image. (b), (c) The SEM images of a Au-nanospheres decorated fiber probe surface at varied magnifications, respectively. (d) Typical TEM image of the Au nanospheres used for decoration of the fiber probe.

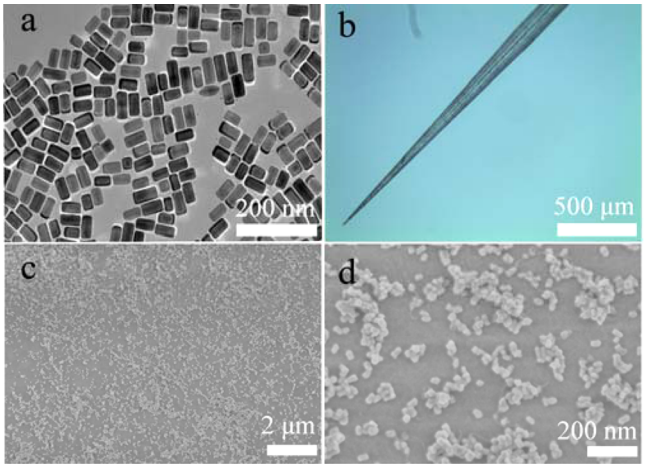

Figure 4. (a) TEM image of positively charged CTAC stabilized Au@Ag core−shell nanorods used for the decoration of fiber tips. (b) The optical image of Au@Ag core−shell nanorods assembled on a 8.2° tapered fiber probe using CEOS as the silane couple agent. (c), (d) The SEM images of Au@Ag core−shell nanorods decorated fiber probe surfaces at varied magnifications, respectively.

persed Au@Ag core−shell nanorods (8.4 nm Ag shell, Figure 4a) that were functionalized with dense CTAC molecules. An important reason we chose this structure is that the SPR of the Au@Ag core−shell nanorods can be readily tuned from 3 to 10 nm by controlling the Ag shell thickness wrapped on the Au-nanorod surface (Figure S3a). In this way a red shift of a longitudinal mode from the Au@Ag core−shell nanorods along with the decrease of the Ag shell thickness is observed (Figure S3b). This structure can be applied in SPR-based sensors.[23] Nevertheless, we concentrated on the SERS performance of the Au@Ag core−shell nanorods. Further Raman measurements indicate that the nanorods with a 8.4 nm Ag shell gave the best SERS sensitivity (Figure S3c) under 785 nm excitation. It should be mentioned, due to the large amount excessive CTAC surfactant in the Au@Ag core−shell nanorods suspensions, the negative charges carried by a CEOS-decorated fiber probe tend to be neutralized when dipped in suspensions of Au@Ag core−shell nanorods. So we applied repeated centrifugation of the Au@Ag core−shell nanorods (or Au-nanorod) suspensions to remove most of the excessive CTAC (or CTAB). In this process, the core−shell nanorods tend to be unstable and aggregate due to the reduced CTAC molecules in the

DOI: 10.1021/acsami.5b04202
ACS Appl. Mater. Interfaces 2015, 7, 17247−17254

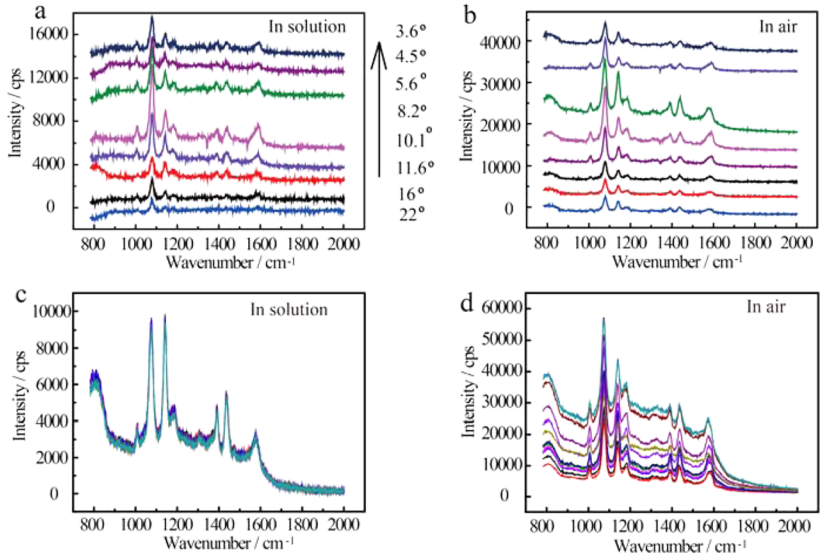

Figure 5. (a), (b) SERS spectra of *p*-ATP (10^{-5} M) adsorbed on a Ag nanocubes sensitized fiber probe with varied cone angles as indicated in the middle of the figure, measured in solution at (a) 20 mW and (b) 10 mW, respectively. (c), (d) Twelve repeated SERS spectra of *p*-ATP (10^{-5} M) adsorbed on a Ag nanocubes assembled fiber probe (8.2°) tested in analyte solution and air, respectively (20 mW).

suspension and on the nanorod surface. As revealed by the optical image in Figure 4b, and SEM images in Figure 4c and Figure 4d, a layer of such a particle cluster has been drawn onto the CEOS-decorated tapered fiber probe from the Au@Ag core−shell nanorods suspension. With this principle of electrostatic attraction, positively charged CTAB stabilized Au-nanorods also can be assembled onto the CEOS-functionalized fiber probe, as shown in Figure S4 in the Supporting Information.

3.3. Effect of cone angle on the SERS sensitivity of the tapered fiber probe. First, we studied the relationship between the SERS activity and the cone angle of the fiber probes. In our experiments, the cone angle of the fiber probe is finely tuned by controlling the up-pulling speed of the fiber from hydrofluoric acid solution. First, it is necessary to investigate the background Raman signals of the system. The dark Raman signals of the fiber without any plasmonic nanostructures hung on are shown in Figure S5. All the SERS spectra were therefore corrected by subtracting the dark Raman scattering noise (the upper curve in Figure S5) generated by the fibers themselves after the standard fiber probe. Figure 5a and Figure 5b present the SERS spectra of *p*-ATP from the Ag-nanocube assembled tapered fiber probes with different eight cone angles from 22° to 3.6°. It is observed that the 8.2° SERS fiber probe shows higher spectral intensities, which might be qualitatively understood as follows. According to optical waveguide theory, with the gradual decrease of fiber diameter in the taper region, the energy of higher order guided wave modes would be transferred into the lower order guided modes or even the radiation wave modes, which is closely related with the cone angles. With the decrease of cone angle, the ratio of radiation wave modes components is lower and the surface area of fiber is enlarged, which means a relatively low transmission loss of the excitation laser and higher excitation efficiency of SERS signals might be achieved.[33] At the same time, the smaller cone angle provides larger numerical aperture, which is also a benefit of the collection of SERS intensity. However, the behavior of the cone angle is not "the smaller the better". When the cone angle is small enough, parts of laser energy would propagate to the end of the fiber taper directly with such a short taper length, which decreases the efficient excitation of the SERS intensity. As a result, the fiber probe with a cone angle at the regime of 8.2° shows excellent Raman signal intensities either in the solution phase sample (Figure 5a) or in the air (Figure 5b).

In the experiments, we noted that, typically for a SERS fiber probe, the SERS intensity is relatively weaker in analyte solution than in the air after a "dip and dry" process. Here the "dip and dry" process means first put the fiber probe in analyte solution for a few seconds (usually ∼20 s) and then manually take the probe out and dry it naturally within a few seconds, since the solvent hung on the probe surface is rather limited. Upon this "dip and dry" procedure, additional analyte molecules from the small volume solution are attached on the SERS probe surface, the medium environment changes (Figure S6a and b), and the analyte molecules may be closer to the nanostructure surface. Thus, the total SERS signal intensities tend to increase due to the combinational effects. In this sense, the dried SERS fiber probes can be applicable for analytes that are hard to adsorb on the fiber surface and improve the detection sensitivity, in addition to the advantages of easy access to microscale environments and minimizing sample handling.[34]

3.4. SERS signal reproducibility of the SERS fiber probes. So far as the nanostructures are attached on the surface of the fiber through electrostatic force, the particles are suspected to disperse in solution; so it is important to evaluate the reproducibility of the SERS fiber probe. First we focused on the signal stability of a single SERS fiber probe exposed in analyte solutions by repeatedly measuring SERS spectra from the same SERS fiber probe. Twelve overlapped SERS spectra of *p*-ATP adsorbed on the same fiber probe (8.2°) recorded successively in Figure 5c shows that the SERS signals are highly reproducible in the analyte solution, indicating that most of the bound nanostructures are difficult to break away. The relative standard deviation (RSD) of SERS signals for the 1079 cm^{-1} shift is 2%.

DOI: 10.1021/acsami.5b04202
ACS Appl. Mater. Interfaces 2015, 7, 17247−17254

Furthermore, we investigated the batch-to-batch (fabricated probes) variability in the SERS signal. For this purpose, we prepared several groups of differently angled tapered fiber probes, each containing seven naked tapered fibers, as shown by the optical images in Figure S7. It was measured that the prepared naked fiber probes show an angle deviation between 0.1° and 0.4°. In this sense, the fabrication of the naked fiber probe is reproducible. Next, the signal reproducibility among different fiber probes of the same angle assembled with Ag nanocubes is evaluated by using *p*-ATP solution (10^{-5} M). We randomly chose a batch of fiber probes with a typical angle of 10.1°. The SERS spectra among varied fiber probes are shown in Figure S8. The RSD of the SERS signals for the 1079 cm^{-1} shift is calculated to be 11.8%. This value is far higher than that from a single fiber probe (RSD ~ 2%). In this sense, the signal reproducibility of the SERS fiber probe is fair.

When dealt with a "dip and dry" process, the SERS (Figure 5d) signal intensities increase and fluctuate significantly as the signal acquisition goes on, possibly attributed to the constant thermal effect of excitation laser. Hence, the RSD value increases to 13.3%. It should be noticed that when the fiber probe is transferred from solution into air, the surface plasmon of the Ag nanocubes is more enhanced with the 785 nm excitation around the Ag nanocubes due to the reduced refractive index of the medium, as testified by the finite element modeling (FEM, Figure S6a and Figure S6b). Thus, the Raman signal intensities of *p*-ATP from the Ag nanocubes assembled fiber probe are improved almost by 4 times when transferred from solution into the air measured at the same laser power of 20 mW.

3.5. SERS sensitivity of the SERS fiber probes. First of all, it is very necessary to compare the enhancement in signal between an untapered fiber and a tapered fiber. For this purpose, we prepared a flat fiber probe by using a cutting knife and decorated it with Ag nanocubes. The SERS spectra are shown in Figure S9. It is observed that the SERS signals from a flat fiber probe are strong but weaker than the 8.2° tapered fiber probe. The intensity difference is more than 3 times. Next, we compared the SERS activity of the above-mentioned four nanostructures-sensitized (Au nanosphere, Ag nanocube, Au nanorod, and Au@Ag core−shell nanorod) fiber probes. Figure 6a presents that, under identical measuring conditions, the Au nanospheres decorated fiber probe (indicated in Figure 3) provides the poorest SERS sensitivity. In contrast, sharp-edged Ag nanocubes and Au@Ag core−shell nanorods assembled fiber probes demonstrate obviously higher spectral intensities for *p*-ATP.

Two combinational reasons can be ascribed to the different sensitivities of the four SERS fiber probes. On one hand, the electromagnetic enhancement generated from the nanostructure varies, as illustrated by the FEM simulations (Figure S6). Generally, large electromagnetic enhancement stems from the nanostructure corners where the free electrons oscillate. Especially for the aggregated Au@Ag nanorods assembled fiber probe, the enhancement is significantly higher due to the electromagnetic coupling effect between neighboring nanorods (Figure S6e). On the other hand, the resonance between the 785 nm excitation line and the surface plasmon of nanostructures is also variant (Figure S10). The absorbance of Au@Ag core−shell nanorods (8.4 nm Ag shell) centering at 610 nm can be partially coupled with the 785 nm laser line. However, for the Au nanospheres, the peak centering at 523 nm is far from the 785 nm. Taken together, the Au@Ag core−shell nanorods show the best SERS activity whereas Au nanospheres perform the worst.

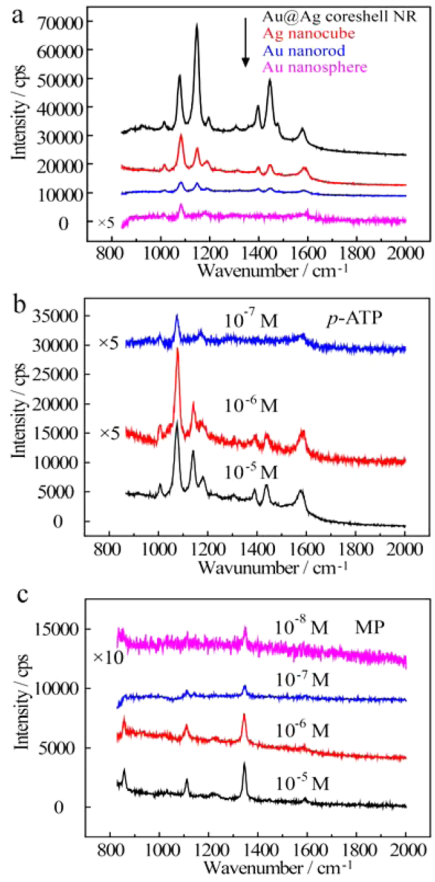

Figure 6. (a) Comparative SERS spectra of *p*-ATP (10^{-5} M) adsorbed on the plasmonic nanostructures sensitized tapered fiber probe. (b) SERS spectra of *p*-ATP with different concentrations adsorbed on the Ag nanocube assembled tapered fiber probe. (c) SERS spectra of MP with varied concentrations adsorbed on the Ag nanocube assembled tapered fiber probe. Here all the fiber probes with 8.2° cone angle are measured in the analyte solution at 20 mW.

Next, the Ag nanocubes sensitized fiber probes were used for the *in situ* detection application, due to the relatively higher uniformity of particle distribution on the fiber surface compared to Au@Au core−shell nanorods. Actually, the detection concentration can be down to 10^{-7} M for *p*-ATP (Figure 6b). Furthermore, the Ag nanocubes sensitized fiber probe was used for the detection of MP, a world-widely used pesticide. Although MP molecules have weak binding affinity toward the Ag surface, they can be adsorbed on the SERS fiber probe surface by the optical gradient force from the 785 nm excitation.[35] Figure 6c shows the SERS spectra of aqueous solutions of MP under different measuring concentrations. Typical SERS fingerprints of MP are observed at 857 cm^{-1} (N═O stretching), 1110 cm^{-1} (phenyl ring C−H wagging), 1343 cm^{-1} (C−N stretching), and 1590 cm^{-1} (phenyl ring stretching), respectively.[36] When the concentration decreases to 10^{-8} M, the strong C−N stretching at 1343 cm^{-1} can be clearly found.

The average enhancement factor of SERS fiber probes can be calculated by the formula $EF = (I_{SERS}/N_{SERS})(I_{RS}/N_{RS})^{-1}$ established by E. C. Le Ru etc.,[37] where I_{SERS} and I_{RS} represent the relative band intensities of the SERS spectrum from a nanoparticles functionalized fiber probe and the Raman

DOI: 10.1021/acsami.5b04202
ACS Appl. Mater. Interfaces 2015, 7, 17247−17254

spectrum (non-SERS) from a naked fiber probe respectively, and N_{SERS} and N_{RS} represent the number of molecules illuminated by the excitation laser. In our experiments, the *p*-ATP molecules can be preconcentrated on the nanoparticle surface through covalent Ag−S or Au−S, whereas the MP molecules do not have strong binding affinity groups toward the silica surface of the fiber probe and the plasmonic nanoparticle surface. So to be fair when deciding the number of adsorbed molecules, we chose MP as the analyte to evaluate the enhancement factor of the SERS fiber probe. We assumed that the volume of analytes near the taper surface (either with or without plasmonic nanostructures) all contributes to the Raman signals. This formula can be deviated as $EF = (I_{SERS}/C_{SERS})(I_{RS}/C_{RS})^{-1}$. We noted that, in the measurements, the normal Raman signals of MP are hard to be acquired at a low concentration (e.g., 10^{-5} M) by a naked fiber probe. So we applied MP with a high concentration of 10^{-2} M to obtain the Raman spectrum as shown in Figure 7a. The main peak at 1345

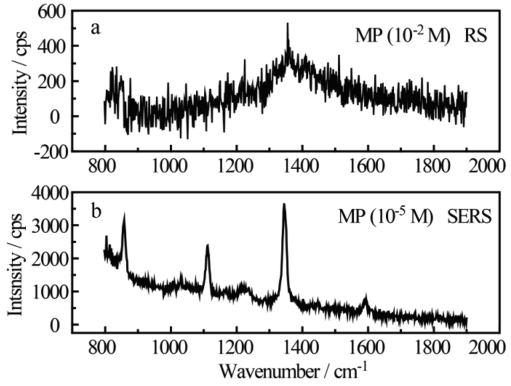

Figure 7. (a) Normal Raman spectrum of MP (10^{-2} M) measured by using a naked 8.2° fiber probe. (b) SERS spectrum of MP (10^{-5} M) measured by using a Ag-nanocube sensitized 8.2° fiber probe. Both spectra were measured in the solution of MP at 20 mW.

cm^{-1} shift is observed. In order to get an authentic but not exaggerated result, we did not use the lower limit of detection concentration; instead, we adopted an MP solution concentration at which the SERS signals can be reproducible, e.g., 10^{-5} M (Figure 7b). An average enhancement factor of 1.6×10^4 was achieved for the optimized 8.2° fiber probe decorated with Ag nanocubes.

4. CONCLUSIONS

In conclusion, we have presented a versatile and reliable approach toward a shape-controlled noble metal nanostructures-sensitized tapered fiber probe for SERS-based detection via reversed charge electrostatic attraction. It is shown that by modifying the fiber probe with silane couple agents of contrary electronegativity, charged (either negative or positive) Ag/Au nanostructures with desired SPR properties can be homogeneously assembled on the surface of the fiber probe. Four nanostructures, Ag nanocubes, Au nanospheres, Au nanorods, and Au@Ag core−shell nanorods with disdinct SPR properties as examples are thereby assembled onto the surface of tapered fiber probes. In addition, the cone angle of the fiber probe was tuned to obtain optimal SERS sensitivity. Besides, *in situ* Raman measurements indicate a detection concentration of methyl parathion down to 10^{-8} M can be realized. The nanostructures-sensitized fiber probe demonstrates good SERS signal stability in analyte solutions, exhibiting potentials in SERS-based *in situ* monitoring of liquid analytes. Furthermore, the concept of coupling shape-controlled nanostructures with the silica surface of a fiber probe via electrostatic attracting opens the door for SPR-related fiber sensors.

■ ASSOCIATED CONTENT

Supporting Information

SEM images, TEM images, SERS spectra, and FEM results of the plasmonic nanostructures, optical images of nanostructure-sensitized tapered fiber probe, and optical absorbance spectra of the nanostructures. The Supporting Information is available free of charge on the ACS Publications website at DOI: 10.1021/acsami.5b04202.

■ AUTHOR INFORMATION

Corresponding Author

*E-mail: gwmeng@issp.ac.cn.

Notes

The authors declare no competing financial interest.

■ ACKNOWLEDGMENTS

We thank the National Key Basic Research Program of China (Grant 2013CB934304), the Natural Science Foundation of China (Grants 51201159, 11274312, and 51472245), and the CAS/SAFEA International Partnership Program for Creative Research Teams for the financial support.

■ REFERENCES

(1) Viets, C.; Hill, W. Comparison of fibre-optic SERS sensors with differently prepared tips. *Sens. Actuators, B* **1998**, *51*, 92−99.

(2) Yang, X.; Gu, C.; Qian, F.; Li, Y.; Zhang, J. Z. Highly Sensitive Detection of Proteins and Bacteria in Aqueous Solution Using Surface-Enhanced Raman Scattering and Optical Fibers. *Anal. Chem.* **2011**, *83*, 5888−5894.

(3) Stokes, D. L.; Vo-Dinh, T. Development of an integrated single-fiber SERS sensor. *Sens. Actuators, B* **2000**, *69*, 28−36.

(4) Yan, M. H.; Chen, J. P.; Jiang, W. N.; Li, J. L.; Chen, J. F.; Li, X. Automatic design scheme for optical-fiber Raman amplifiers backward-pumped with multiple laser diode pumps. *Ieee Photonics Technol. Lett.* **2001**, *13*, 948−950.

(5) Amezcua-Correa, A.; Yang, J.; Finlayson, C. E.; Peacock, A. C.; Hayes, J. R.; Sazio, P. J. A.; Baumberg, J. J.; Howdle, S. M. Surface-enhanced Raman scattering using microstructured optical fiber substrates. *Adv. Funct. Mater.* **2007**, *17*, 2024−2030.

(6) Lucotti, A.; Zerbi, G. Fiber-optic SERS sensor with optimized geometry. *Sens. Actuators, B* **2007**, *121*, 356−364.

(7) Zhu, Y.; Dluhy, R. A.; Zhao, Y. Development of silver nanorod array based fiber optic probes for SERS detection. *Sens. Actuators, B* **2011**, *157*, 42−50.

(8) Smythe, E. J.; Dickey, M. D.; Bao, J. M.; Whitesides, G. M.; Capasso, F. Optical Antenna Arrays on a Fiber Facet for in Situ Surface-Enhanced Raman Scattering Detection. *Nano Lett.* **2009**, *9*, 1132−1138.

(9) Liu, T.; Xiao, X.; Yang, C. Surfactantless Photochemical Deposition of Gold Nanoparticles on an Optical Fiber Core for Surface-Enhanced Raman Scattering. *Langmuir* **2011**, *27*, 4623−4626.

(10) Zheng, X.; Guo, D.; Shao, Y.; Jia, S.; Xu, S.; Zhao, B.; Xu, W.; Corredor, C.; Lombardi, J. R. Photochemical modification of an optical fiber tip with a silver nanoparticle film: A SERS chemical sensor. *Langmuir* **2008**, *24*, 4394−4398.

(11) Fan, Q.; Cao, J.; Liu, Y.; Yao, B.; Mao, Q. Investigations of the fabrication and the surface-enhanced Raman scattering detection applications for tapered fiber probes prepared with the laser-induced chemical deposition method. *Appl. Opt.* **2013**, *52*, 6163−6169.

DOI: 10.1021/acsami.5b04202
ACS Appl. Mater. Interfaces 2015, 7, 17247−17254

(12) Urban, A. S.; Shen, X.; Wang, Y.; Large, N.; Wang, H.; Knight, M. W.; Nordlander, P.; Chen, H.; Halas, N. J. Three-Dimensional Plasmonic Nanoclusters. *Nano Lett.* **2013**, *13*, 4399−4403.
(13) Mulvihill, M.; Tao, A.; Benjauthrit, K.; Arnold, J.; Yang, P. Surface-enhanced Raman spectroscopy for trace arsenic detection in contaminated water. *Angew. Chem., Int. Ed.* **2008**, *47*, 6456−6460.
(14) Frens, G. CONTROLLED NUCLEATION FOR REGULATION OF PARTICLE-SIZE IN MONODISPERSE GOLD SUSPENSIONS. *Nature, Phys. Sci.* **1973**, *241*, 20−22.
(15) Xia, Y.; Xiong, Y.; Lim, B.; Skrabalak, S. E. Shape-Controlled Synthesis of Metal Nanocrystals: Simple Chemistry Meets Complex Physics? *Angew. Chem., Int. Ed.* **2009**, *48*, 60−103.
(16) Zhang, Q.; Li, W.; Wen, L.-P.; Chen, J.; Xia, Y. Facile Synthesis of Ag Nanocubes of 30 to 70 nm in Edge Length with CF_3COOAg as a Precursor. *Chem. - Eur. J.* **2010**, *16*, 10234−10239.
(17) Panfilova, E.; Shirokov, A.; Khlebtsov, B.; Matora, L.; Khlebtsov, N. Multiplexed dot immunoassay using Ag nanocubes, Au/Ag alloy nanoparticles, and Au/Ag nanocages. *Nano Res.* **2012**, *5*, 124−134.
(18) Sau, T. K.; Murphy, C. J. Seeded high yield synthesis of short Au nanorods in aqueous solution. *Langmuir* **2004**, *20*, 6414−6420.
(19) Scarabelli, L.; Coronado-Puchau, M.; Giner-Casares, J. J.; Langer, J.; Liz-Marzan, L. M. Monodisperse Gold Nanotriangles: Size Control, Large-Scale Self-Assembly, and Performance in Surface-Enhanced Raman Scattering. *ACS Nano* **2014**, *8*, 5833−5842.
(20) Khoury, C. G.; Vo-Dinh, T. Gold Nanostars For Surface-Enhanced Raman Scattering: Synthesis, Characterization and Optimization. *J. Phys. Chem. C* **2008**, *112*, 18849−18859.
(21) Niu, W. X.; Xu, G. B. Crystallographic control of noble metal nanocrystals. *Nano Today* **2011**, *6*, 265−285.
(22) Jin, R. C.; Cao, Y. W.; Mirkin, C. A.; Kelly, K. L.; Schatz, G. C.; Zheng, J. G. Photoinduced conversion of silver nanospheres to nanoprisms. *Science* **2001**, *294*, 1901−1903.
(23) Zeng, S.; Baillargeat, D.; Ho, H.-P.; Yong, K.-T. Nanomaterials enhanced surface plasmon resonance for biological and chemical sensing applications. *Chem. Soc. Rev.* **2014**, *43*, 3426−3452.
(24) Zhang, C.-L.; Lv, K.-P.; Huang, H.-T.; Cong, H.-P.; Yu, S.-H. Co-assembly of Au nanorods with Ag nanowires within polymer nanofiber matrix for enhanced SERS property by electrospinning. *Nanoscale* **2012**, *4*, 5348−5355.
(25) Zheng, J. W.; Zhu, Z. H.; Chen, H. F.; Liu, Z. F. Nanopatterned assembling of colloidal gold nanoparticles on silicon. *Langmuir* **2000**, *16*, 4409−4412.
(26) Nakamura, Y.; Yamazaki, R.; Fukuda, T.; Shitajima, K.; Fujii, S.; Sasaki, M. Structure of silane layer formed on silica particle surfaces by treatment with silane coupling agents having various functional groups. *J. Adhes. Sci. Technol.* **2014**, *28*, 1895−1906.
(27) Thompson, W. R.; Cai, M.; Ho, M. K.; Pemberton, J. E. Hydrolysis and condensation of self-assembled monolayers of (3-mercaptopropyl)trimethoxysilane on Ag and Au surfaces. *Langmuir* **1997**, *13*, 2291−2302.
(28) Seo, D.; Park, J. C.; Song, H. Polyhedral gold nanocrystals with O-h symmetry: From octahedra to cubes. *J. Am. Chem. Soc.* **2006**, *128*, 14863−14870.
(29) Xiong, Y.; Washio, I.; Chen, J.; Cai, H.; Li, Z.-Y.; Xia, Y. Poly(vinyl pyrrolidone): A dual functional reductant and stabilizer for the facile synthesis of noble metal nanoplates in aqueous solutions. *Langmuir* **2006**, *22*, 8563−8570.
(30) Gole, A.; Murphy, C. J. Seed-mediated synthesis of gold nanorods: Role of the size and nature of the seed. *Chem. Mater.* **2004**, *16*, 3633−3640.
(31) Okuno, Y.; Nishioka, K.; Kiya, A.; Nakashima, N.; Ishibashi, A.; Niidome, Y. Uniform and controllable preparation of Au-Ag core-shell nanorods using anisotropic silver shell formation on gold nanorods. *Nanoscale* **2010**, *2*, 1489−1493.
(32) Su, Q.; Ma, X.; Dong, J.; Jiang, C.; Qian, W. A Reproducible SERS Substrate Based on Electrostatically Assisted APTES-Functionalized Surface-Assembly of Gold Nanostars. *ACS Appl. Mater. Interfaces* **2011**, *3*, 1873−1879.
(33) Guo, S. P.; Albin, S. Transmission property and evanescent wave absorption of cladded multimode fiber tapers. *Opt. Express* **2003**, *11*, 215−223.
(34) Pesapane, A.; Lucotti, A.; Zerbi, G. Fiber-optic SERS sensor with optimized geometry: testing and optimization. *J. Raman Spectrosc.* **2010**, *41*, 256−267.
(35) Chang, R. L. Optical force acting on a molecule near a metal sphere: effects of decay rate change and resonance frequency shift. *Opt. Commun.* **2005**, *249*, 329−337.
(36) Huang, Z.; Meng, G.; Huang, Q.; Chen, B.; Zhou, F.; Hu, X.; Qian, Y.; Tang, H.; Han, F.; Chu, Z. Polyacrylic acid sodium salt film entrapped Ag nanocubes as molecule traps for SERS detection. *Nano Res.* **2014**, *7*, 1177−1187.
(37) Le Ru, E. C.; Blackie, E.; Meyer, M.; Etchegoin, P. G. Surface Enhanced Raman Scattering Enhancement Factors: A Comprehensive Study. *J. Phys. Chem. C* **2007**, *111*, 13794.

DOI: 10.1021/acsami.5b04202
ACS Appl. Mater. Interfaces 2015, 7, 17247−17254